Sensors & Actuators: A. Physical 396 (2025) 117095

Contents lists available at ScienceDirect

Sensors and Actuators: A. Physical

journal homepage: www.journals.elsevier.com/sensors-and-actuators-a-physical

Magnetic nanoparticle spectroscopy for multiplex detection: Insights from frequency mixing magnetic detection

Ali Mohammad Pourshahidi [b], Jae Chan Jeong [a], Hans-Joachim Krause [b], Hyo Bong Hong [a,*]

[a] Electronics and Telecommunications Research Institute (ETRI), 218 Gajeong-ro, Yuseong-gu, Daejeon, Republic of Korea
[b] Institute of Biological Information Processing, Bioelectronics (IBI-3), Forschungszentrum Jülich, Jülich 52425, Germany

A B S T R A C T

Magnetic nanoparticles (MNPs) have shown promising applications in the field of biomedical sciences. Subsequently, various types of Magnetic Particle Spectroscopy (MPS) have been proposed for quantitative and qualitative analysis of MNPs. Among the various functions of MPS proposed so far, the development of technology that can analyze multiplex detection of different types of MNPs has attracted due to the expansion of various application fields. For example, the technology can be applied to enhance efficiency in biosensors, process analysis in MNP manufacturing, and measurement of various diseases in MPI. In our investigation, we perform a comparative study of different commercially available MNPs for use in multiplex detection applications using the frequency mixing magnetic detection (FMMD) technique. In this method, we employ a low-frequency magnetic field scanning method and analyze the real and imaginary parts of the measurement signal $f_1 + 2 \cdot f_2$ obtained from binary mixture samples of different MNP type combinations. Our findings suggest that FMMD-based duplex detection can achieve effective and reliable differentiation when a substantial phase response deviation exists among the particles.

1. Background

Magnetic nanoparticles (MNPs) have gained significant attention in recent years for their versatile use in diagnostics [1–3], imaging as contrast agents in magnetic resonance imaging (MRI) and as tracers in magnetic particle imaging (MPI) [4–7]. Moreover, they are used as therapeutic interventions specifically in magnetic fluid hyperthermia [8–10]. Another important application of MNPs in biomedical research field is their use as markers in biosensing [11–13]. A key advantage of MNP-based biosensing techniques lies in their distinct magnetic signatures, which make them suitable for sensitive detection with minimal background interference. In liquid samples, these signatures arise from the nonlinear magnetization of MNPs and their relaxation dynamics, predominantly Brownian and Néel processes, which imprint characteristic amplitudes and phases on driven magnetic responses [14,15]. The relaxation times depend on different properties, such as core and hydrodynamic size from the particle properties side, and on environmental factors such as viscosity and temperature. These parameters can shape the measured spectral features. Recent advancements in magnetic particle spectroscopy and related techniques have focused on improving measurement sensitivity, robustness, and versatility through innovations in both detection strategies and hardware design. Studies have introduced optimized harmonic analysis methods, low-cost and portable instrumentation [16–18], novel sensing metrics [19], and advanced modeling approaches for parameter estimation, such as temperature sensing based on Brownian relaxation dynamics [20]. These developments show the continuous effort to enhance magnetic nanoparticle-based measurement systems for applications ranging from sensitive biosensing to complex environmental and biomedical diagnostics [3,21]. One particularly promising area of development is in multiplex detection, where different types of MNPs can be used simultaneously to detect multiple analytes, thereby providing a more comprehensive analysis compared to traditional single-target methods [22]. This approach is particularly valuable in complex diagnostic scenarios such as simultaneous detection of different biomarkers, analysis of the MNP production process, where size and composition vary depending on the synthetic reaction, and analysis of biogenic MNPs produced according to metabolic activity [23–26].

Most of the multiplex methods proposed in previous studies to date immobilize the analyte or MNP on the platform or separate the particles through floe fracturing before analysis. While this can be very effective in an array-type biosensing system, it is not suitable for analyzing the mixed samples mentioned above and often requires a separate separation system. To overcome this problem, studies have been conducted on a multiplexing method that relies on MPS measurements where the response signal of MNP subjected to alternating magnetic field is analyzed. In a study using magnetic spectroscopy of Brownian motion, Rauwerdink et al. showed that three different MNPs could be analyzed

* Corresponding author.
E-mail address: hb8868@etri.re.kr (H.B. Hong).

https://doi.org/10.1016/j.sna.2025.117095
Received 13 June 2025; Received in revised form 17 August 2025; Accepted 24 September 2025
Available online 9 October 2025

simultaneously up to the fraction, but all the samples used in this experiment were fixed using epoxy [27]. Techniques like magnetic relaxation and magnetic susceptibility measurements have been used for in biosensing applications primarily for individual biomarkers detection [17,28–32] with limited demonstrated capability for simultaneous, quantitative multiplex analyses. Moreover, in the recent advancements for multiplex detection strategies, the Frequency Mixing Magnetic Detection (FMMD) technique has shown promise for distinction of the magnetic signatures of different types of MNPs, based on the phase response [33,34] and characteristic features identified by scanning either the static offset field [35] or by modulating low-frequency magnetic fields [36]. Another practical advantage of FMMD in analyzing MNP mixtures is that the measured phase-based features at selected mixing harmonic products can be comparatively less concentration dependent than the amplitudes [34,35]. Moreover, another advantage of this technique lies in its sensitivity and specificity to the superparamagnetic behavior inherent to MNPs, making it suitable for real-time multiplexed analysis in complex fluidic samples. Despite this potential, there is currently limited systematic evaluation of commercially available MNPs, leaving significant uncertainty about which particle combinations yield optimal performance for practical duplex detection scenarios. In addition, selection criteria for particle pairs, such as simple separability metrics, recommended operating window for the frequency and field, and robustness to viscosity or temperature drift—are not yet standardized for free-solution measurements. Important practical questions therefore remain open: How well can commonly used particles be distinguished using phase-centered FMMD features, and which combinations of particle types provide stable separation across these variations without requiring immobilization or additional sample preparation.

Hence a comparative study is required to assess the performance of commercially available and frequently used MNPs within duplex detection framework. This study aims to evaluate the feasibility of duplex detection using different commercially available MNPs. We compare the complex real and imaginary part (in-phase and quadrature) signatures at selected FMMD mixing harmonic ($f_1+2\cdot f_2$) for duplex discrimination. By comparing the magnetic response of different MNPs types and their combinations, this work seeks to identify suitable pairs of nanoparticle types that can be used in future multiplexed assays. Our results contribute directly to advancing the FMMD technique as a reliable measurement platform for multiplex biosensing applications. Hence, e expected to lay the groundwork practical implementations in biomedical diagnostics as well as magnetic particle imaging (MPI), specifically FMMD-MPI applications [37].

2. Methods

2.1. Frequency mixing magnetic detection

FMMD is a technique that utilizes nonlinear magnetic responses to detect magnetic nanoparticles under the influence of two simultaneously applied alternating excitation magnetic fields of different frequencies [38]. Due to the nonlinear magnetization response of the magnetic nanoparticles, new intermodulation components (sum and difference frequencies) are generated. These mixed frequency components are detected and allow identification and quantification of different types of magnetic nanoparticles. The excitation field is of the form

$$B(t) = B_0 + B_1 \sin(2\pi f_1 t) + B_2 \sin(2\pi f_2 t). \quad (1)$$

where B_0 is the static offset magnetic field, and B_1 and B_2 are the amplitudes of the high and low frequency magnetic fields with frequencies f_1 and f_2, respectively. In presence of magnetic nanoparticle samples, the response signal will contain mixing harmonics of interest ($f_1+n\cdot f_2$, $n = 1, 2, 3$ …) due to the nonlinearity of their magnetization, that are further analyzed. In the absence of static offset magnetic field, the magnetization curve remains point-symmetric; even-order terms average to zero. Hence, intermodulation products that contain odd integer multiples of f_2 ($n = 1,3,5.$) like f_1+f_2 or $f_1+ 3\cdot f_2$ are cancelled, while the third-order $f_1+ 2\cdot f_2$ term survives and is the dominant detectable sideband [38].

For monodispersed particles with magnetic moment $\mu = M_s V_c$, the magnetization in equilibrium is typically modeled by the so-called Langevin function

$$M_{eq}(t) = \mu L(\xi(t)), \xi(t) = \frac{\mu B(t)}{k_B T}. \quad (2)$$

For small ξ values we use $L(\xi) = \frac{\xi}{3} - \frac{\xi^3}{45} + \ldots$, inserting the field B(t) from (1) and collecting the cubic terms, showing that the $f_1+ 2\cdot f_2$ component scales as follows

$$S_{f_1+2\cdot f_2} \propto \frac{\mu^4}{(k_B T)^3} B_1 B_2^2 \mathscr{T}_3(\xi_{rms}), \quad (3)$$

where $\mathscr{T}_3(\xi_{rms})$ is the effective third order Langevin factor which is essentially the third derivative of the Langevin function.

Thus, at low excitation field amplitude B_2, the response scales as $S_{f_1+2\cdot f_2} \sim B_1 B_2^2$ (quadratic growth). At large B_2, the Langevin function reaches saturation, so the effective cubic susceptibility decreases, and the $f_1+ 2\cdot f_2$ component declines despite increasing field.

2.2. Experimental setup

The measurement setup used for the experiments involves a FMMD-based magnetic reader that generates the excitation signals, reads out the response signal from the detection coil and transfers the digitized data to a PC using an FPGA protocol. Fig. 1 presents the architecture of this FMMD-based magnetic reader. The FPGA manages four Direct Digital Synthesizers (DDS), Digital-to-Analog Converters (DAC), and a multiplexer (MUX) for signal selection. Additionally, it digitizes analog signals using three Analog-to-Digital Converters (ADC) and transmits the data to the PC. By controlling the DDS and DAC, the system applies a user-defined AC current to the excitation and driver coils, generating the desired excitation magnetic fields. The output signals from the excitation and driver DDS pass through current-amplifying operational amplifiers (OPAMPs) to supply current to the coils. These output signals are attenuated by a factor of 1/10, looped back, and monitored via ADC#2 and ADC#3. The induced voltage from the detection coil is pre-amplified and transmitted to the PC via ADC#1.

The synchronization of each DDS is controlled by a reset signal managed by the microcontroller. A trigger signal for phase detection is generated by the driving DDS and transmitted to the PC through ADC#3. This trigger signal determines the point of frequency analysis in the detection coil signal. The MUX is located in front of ADC#3, enabling the selection between the loop-back signal and the trigger signal. The system is powered by a 24 V, 120 W switching mode power supply (SMPS), delivering ±18 V to the current-amplifying OPAMPs and ±5 V for the DDS, DAC, and ADC.

The excitation fields were characterized using a GM08 Gaussmeter from Hirst magnetic instruments (Falmouth, United Kingdom). To perform the measurements by low frequency amplitude variation, the amplitude of the excitation field is varied within a desired range. The applied settings used in our experiment are listed in Table I.

Performing a Discrete Fourier Transform (DFT) on the digitized signal allows the measurement of the desired mixing harmonics (i.e. f_1+f_2, $f_1+2\cdot f_2$, $f_1+3\cdot f_2$ and $f_1+4\cdot f_2$). The real and imaginary (in-phase and out-of–phase quadrature) components of the mixing frequency terms are measured and analyzed.

2.3. Magnetic nanoparticles

In this study, we utilized several different commercially available

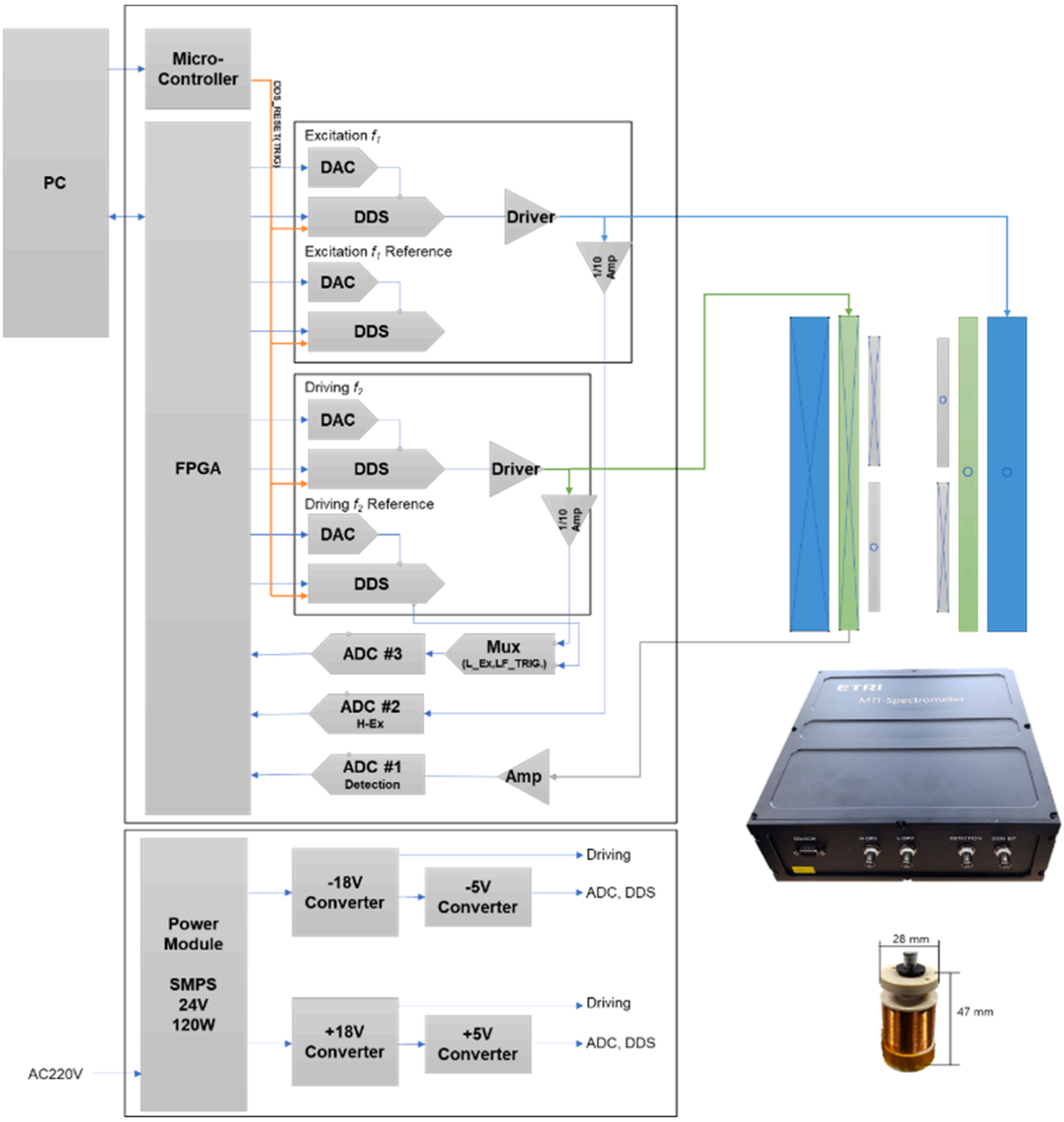

Fig. 1. Left: architecture of the FMMD based magnetic reader device, top right: photograph of the system, and bottom right: photograph of the measurement head, with its dimensions indicated.

Table I
Parameters of the excitation setup.

Excitation field	Magnitude	Frequency
Low-frequency (B_2)	0–17.6 mT / 25 steps	40 Hz
High-frequency (B_1)	0.8 mT	4 kHz

MNPs from companies Micromod Partikeltechnologie GmbH, Rostock, Germany (Micromod) and Ocean Nanotech, San Diego, CA, U.S.A. (Ocean), a list of which is given in Table II.

2.4. Duplex detection strategy and sample preparation

To ensure uniform concentration across different particle types, all samples were initially diluted to a concentration of 5 mg/mL. In the first approach, we characterized different particle types alone using a low frequency (B_2) amplitude scanning approach described in [36].

Particle types exhibiting clearly distinguishable signals were then selected for performance assessment in duplex detection. These binary mixtures were prepared by pipetting and mixing the two constituents with varying ratios in the sample vials.

For both pure and mixture samples, 100 μL of solution were pipetted

Table II
List of the evaluated commercially available magnetic nanoparticles.

No.	Particle name	Hydrodyna-mic size [nm]	Stock concentration [mg/mL]	Surface	Manufacturer
1	SynomagD	50	20	Dextran	Micromod
2	SynomagD	70	20	Dextran	Micromod
3	SynomagS	100	20	Dextran	Micromod
4	Perimag	130	25	Dextran	Micromod
5	NanomagD	250	25	Dextran	Micromod
6	SPA30	30	5	Polymer	Ocean
7	SHP15	15	5	carboxylic acid	Ocean
8	SHP30	30	5	carboxylic acid	Ocean

into 31 mm × 6 mm flat-bottomed, 300 μL glass inserts for HPLC vials. The total volume of 100 μL was chosen to fully match the geometrical height of the detection coil.

2.5. Assessment of the particle contributions

In this work, we adopt an empirical data-oriented approach to evaluate the contributions in the mixtures. In this strategy, we measure reference samples belonging to each of the involved particle types. We assume that the magnetic signal of the mixture of two particle types is a linear combination of the reference measurements of the two constituents, as expected for non-interacting particles. In the duplex particle analysis, this means a summation of the signals of pure particle types A and B multiplied by positive coefficients α and ß. This is performed using a least square approach that minimizes the cost function

$$\min_{\alpha_i,\beta_i} \sum \left[\left(\left(\alpha \cdot A^i_{\mathrm{Re}} + \beta \cdot B^i_{\mathrm{Re}}\right) - M^i_{\mathrm{Re}} \right)^2 + \left(\left(\alpha \cdot A^i_{\mathrm{Im}} + \beta \cdot B^i_{\mathrm{Im}}\right) - M^i_{\mathrm{Im}} \right)^2 \right] \quad (4)$$
$$\alpha_i \geq 0 \quad \text{and} \quad \beta_i \geq 0$$

Here the real and imaginary parts of the measurements of the two pure particle types are denoted as A_{Re}, B_{Re}, A_{Im} and B_{Im}, respectively. The complex parts of the measured signal of the mixture are denoted as M_{Re} and M_{Im}. The process iterates over the varying fields i. This approach was implemented using a python code that utilizes the NNLS solver from the SciPy library.

3. Results and discussion

The 8 different pure particle samples listed in Table II were measured by low-frequency magnetic field amplitude scanning. Due to the absence of a static offset field, the mixing components f_1+f_2 and $f_1+3\cdot f_2$ almost yield no response. The mixing component $f_1+2\cdot f_2$ was substantially stronger than $f_1+4\cdot f_2$ and was therefore studied in the following. The amplitude response and the complex plane representation of the measured mixing frequency harmonic $f_1+2\cdot f_2$ are shown in Fig. 2. The measurements start by changing the amplitude of the low-frequency field (B_2) from 0 to 17.6 mT in 25 steps, as seen in the amplitude response graph (Fig. 2a). The particle response at the second mixing harmonic gradually increases and, depending on the particle type, reaches a maximum at type-dependent excitation field before it decays again. On the complex plane including the phase information, this portraits a hook shape pattern [36]. Since the sample SHP15 showed a linear phase response (see the orange curve in the inset of Fig. 2b), we performed a phase rotation for all the measurements relative to the slope of SHP15. The rotation removes arbitrary instrument phase offsets and allows direct, pairwise comparison of phase trends across particle types.

Based on the obtained results, we can see a good separability among the measured particles. These findings address our initial goal of identifying particle pairs with stable separability and outlining simple selection rule for pair choice. It is well known [33] that a wider difference in measured phase among different particle types will provide grounds for better distinguishability performance. For example, we can see that the particles SPA30 and Syn50 are showing a very similar phase response, but there is a significant difference when comparing them to the particle type Syn70. On the other hand, one has to consider the amplitude response of the particles, since the particles with higher amplitude response usually dominate the measured mixture signals. This can be attributed to the larger effective magnetic moments and relaxation behavior. This can be overcome by adjusting the concentrations, so that the amplitude responses from all the particle types are comparably large. In this study, however, we aimed only at similar concentrations. Hence, selection of the particles for duplex detection evaluation was based on how well separated their signals are in the

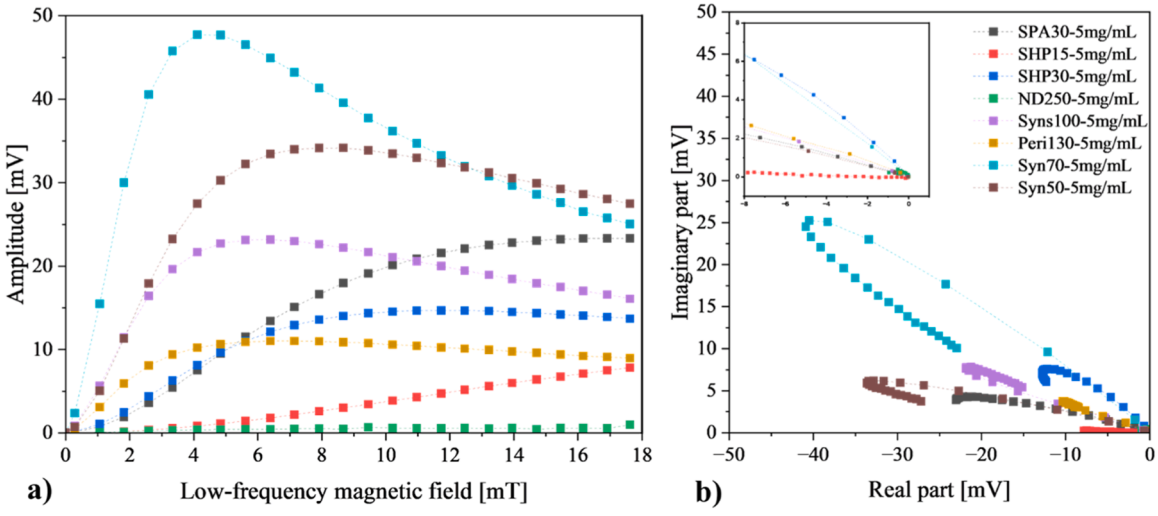

Fig. 2. a) Amplitude response of different magnetic nanoparticle types at mixing frequency harmonic $f_1+2\cdot f_2$ to varying low-frequency magnetic field. b) Complex plane representation of the measurement signals of different MNP types to varying low-frequency magnetic field.

complex plane (meaning the difference in the phase response). It is also noteworthy that the direction of the opening of the hook pattern, observed in the complex plot shown in Fig. 2b, varies among the particles. The majority of the particles show left-sided turns, whereas the particles Syns100 and Peri130 show right-sided turns. The reason behind this observation has been further evaluated in a more theoretical context [39], which is out of the scope of this study. Binary mixture samples consisting of two different particle types were prepared according to Table III.

The complex plots of $f_1+2{\cdot}f_2$ measurement signals for the combination of different particles, as listed in Table III, are presented in Fig. 3. Here, the combo names a.f correspond to the sub-Fig. 3a.3f. The mixing ratios of the two particle types used in the mixtures have been color-coded and are shown in the legend of each graph. In each graph, the measurements related to pure particle A are depicted as black symbols, and measurements related to particle B are shown as blue-gray symbols. The intermediate ratios are shown as spectrum of colors. For example, in Fig. 3a, different mixture ratios of Syn50 and Syn70 are presented, and the basic label for the mixture reads S5070. The following digits show the ratio of each particle type in the mixture. For example, S5070–9–1 indicates that there the sample was made using 90 % Syn50 (particle A) and 10 % Syn70 (particle B). From a qualitative perspective, in all of the cases we can observe that the measured mixture signals lie between the signals of the two pure particle samples. In case of SHP particles, the combination of the 15 and 30 nm type presented in Fig. 3e shows nicely the transition between the two references. The linear response of the 15 nm sample is gradually changing its curvature, which in the end transforms into a hook-shaped pattern. The intermediate ratios are clearly separated from each other in larger magnetic fields. The same effect is also observed in the mixture of SHP 15 nm and Perimag 130 nm (OP15130), however, we can see that, as the ratio of the mixture passes 5:5 and the amount of Perimag particles increases in the mixture, the phase shift between the sample gets smaller, although the shape of the curvature is still evolving (i.e. the curvature of the hook). Moreover, in the results of the mixture of Perimag 130 with SHP 30 nm, we can see that since the phase difference is not as large as the one with SHP 15 nm, there is a good separation among different ratios with a narrower corridor of distinction. As mentioned earlier, Syns100 shows a right-sided hook shape. In the mixture with the Syn70 particle, we can see that the opening of the hook narrows down and gradually the orientation of the hook shifts to the left. However, the phase shift of the signal is mainly dominated by the very large signal of Syn70 particles. In contrast, in the results of the mixtures Syns100 and Syn50, the phase shift is clearly observable. Although the complex plots show both amplitude and phase information, the field amplitude information is not accessible. Therefore, individual amplitude and phase plots are given in the supplement, figure S1.

The measurement data was analyzed with a Python code to estimate the contributions of each particle type based on the measured references that contain 100 % of the particle type of interest. The results are presented in the form of percentage of the respective reference in Fig. 4. The combinations are presented one after each other. For each particle combo, there are two boxes that indicate the estimated percentages of references A and B. The horizontal axis shows the ideal expected values that were used to prepare the samples. The qualitative trend is shown as a color gradient, with red showing the highest percentage and blue the lowest. The actual determined percentages of each particle type are written in the respective boxes. The combinations are highlighted according to the given sample names on the left side of the figure.

The qualitative analysis shows a consistent agreement between the experimentally determined mixture ratios and the expected trends across most MNP combination samples, except for the combination S70100. The observed deviation in this particular pair can be attributed mainly to the large difference in the amplitude responses of the two constituents, the domination of Syn70 in the measured signals has led to this effect, once again highlighting the importance of approximately equal particle contributions in the mixture signals. For quantitative assessment of the deviation of reconstructed mixing ratio from the real one, we quantitatively analyzed the average deviation across all the binary ratios. We found that the mixtures SHP1530 (2.83 %) showed the lowest average total deviation. The combinations S50100 (4 %), OP30130 (5.6 %) and S5070 (6.6 %) have shown slightly larger deviations. Part of the deviations are expected to be due to statistical errors during sample preparation but the impact of possible interactions among the two particle types could also play a role and it remains important to further investigate their influence on the measured signals.

Our finding align and expand with respect the previous studies [40], where the M-H response of particles was utilized for a mathematical study of a multiplex detection strategy, also highlights that selection of particle types which can be combined together is a critical factor in enabling multiplex detection platforms. Our results extends this understanding by explicitly demonstrating the practical comparison of several commercially available particles widely utilized in magnetic biosensing field. Moreover, in such applications it's important to choose the MNPs not just for their individual magnetic properties, but also for how well they respond together in a multiplex setting. The analysis of the combined response in a characterization stage is key to achieving reliable detection. Following the magnetic biosensing emerging strategies that aims to perform wash free bioassays [17,36] in liquid suspensions, our FMMD-based measurements were similarly performed in liquid state to reflect realistic scenario involving freely suspended MNPs. However, as these strategies rely of Brownian relaxation phenomena which manifest as phase shifts in the FMMD signal, a more detailed investigation is required to fully characterize the influence of particle dynamics and fluidic environments. This should include examining the impact of hydrodynamic changes or partial immobilization on the duplex and multiplex detection strategies to ensure robust and reliable performance.

Table III
List of particle mixture combinations.

Combo name	Particle A	Particle B	Mixture name
a	Syn50	Syn70	S5070
b	SHP30	Peri130	OP30130
c	Syn70	Syns100	S70100
d	SHP15	Peri130	OP15130
e	SHP15	SHP30	SHP1530
f	Syn50	Syns100	S50100

4. Conclusion

This work aimed to evaluate duplex detection in liquid suspension using FMMD, to identify suitable pairs among commercially available MNPs, and to give simple selection criteria for practical use. Different commercially available magnetic nanoparticle types that are frequently used for magnetic biosensing and MPI were measured using the FMMD technique. The complex real (in-phase) and imaginary (quadrature) response of the MNPs were measured at the mixing harmonic $f_1+2{\cdot}f_2$ by modulation of the low-frequency magnetic field amplitude (B_2). Analysis of the measurement signals $f_1+2{\cdot}f_2$ from different particles shows that the resulting hook plots in the complex plane show significant differences that can be used for duplex detection. Based on the expressed features, binary mixtures of different types of particles were prepared to evaluate their performance for duplex and multiplex detection. From the comparison study of the different MNP samples, we conclude that good duplex performance based on the studies approach requires (a) a clear phase separation in the complex plane between the two particle types, and (b) comparable amplitude levels so that one particle does not dominate the mixture signal. These practical points translate the observed complex-plane behavior at $f_1+2{\cdot}f_2$ into guidelines for selecting particles and setting concentrations.

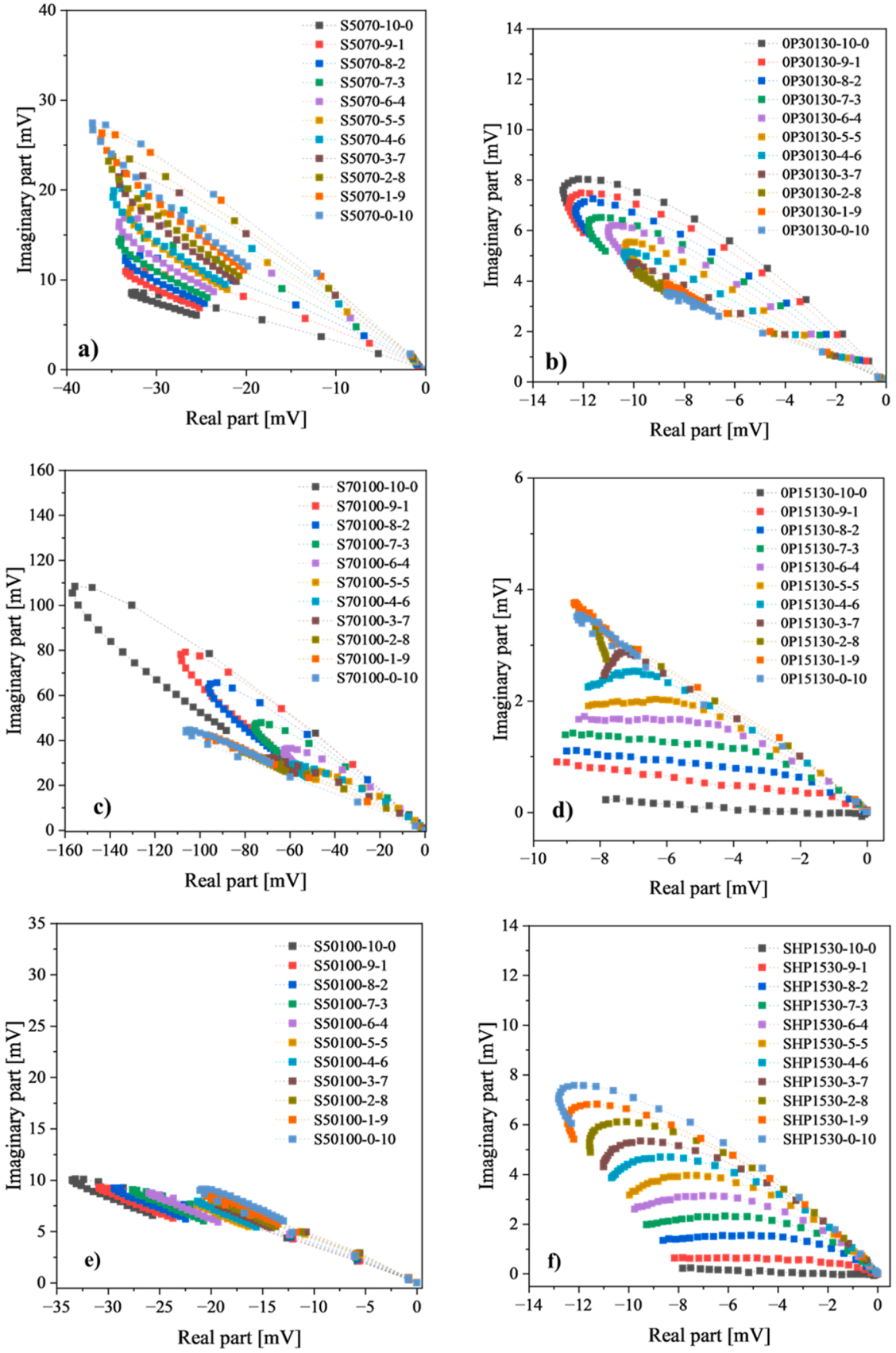

Fig. 3. Measurements of ranges of binary mixture ratios for different particle combinations, as listed in Table III, at mixing harmonic $f_1 + 2 \cdot f_2$ with varying low-frequency magnetic field presented in complex plane. a) Combination of Syn50 and Syn70 (S5070) b) SHP30 and Perimag 130 (OP30130), c) Syn 70 and Syns100 (S70100), d) SHP15 and Perimag 130 (OP15130), e) SHP 15 and SHP 30 (SHP1530) and f) Syn50 and Syns100 (S50100).

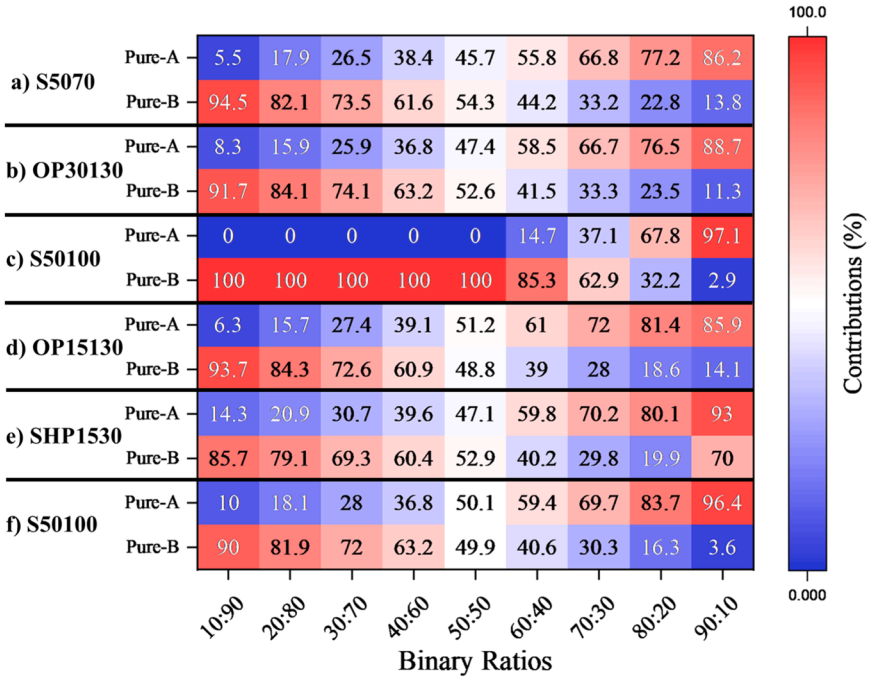

Fig. 4. The estimated contributions of references from particle types A and B in every combination. The Gradient between Red and Blue color indicated the percentage. The estimated percentage of each reference is given in its respective box and compared to the expected ratio on horizontal axis of the graph.

The results showed that mixture ratio extraction is feasible by determining the contributions of each particle type to the measured signal. Except for one combination (Syn70 and Syns100), the general trend strongly agreed with the expected trend, and the reconstructed mixing ratios exhibited only small deviations from the real ratios. The lowest average deviation was observed for the combination of SHP15 and SHP30 which amounted to only 2.83 %. The other mixtures showed errors below 10 % in mixing ratio reconstruction. The identified pairs (in particular SHP15/SHP30, and also S50100, OP30130, S5070) are promising for liquid based wash-free biosensing, and candidates for multi-tracer FMMD-MPI concepts.

In future work, we aim to study the impact of hydrodynamic size variation and of environmental factors such as viscosity on duplex readout. We plan to extend the analysis to triplex mixtures and explore additional mixing components to further improve the results. Additionally, we aim to leverage our insights from this study to further advance the FMMD-MPI technology to distinguish multiple particle types within the reconstructed images.

Author Statement

- the work described has not been published previously except in the form of a preprint, an abstract, a published lecture, academic thesis or registered report.
- the article is not under consideration for publication elsewhere.
- the article's publication is approved by all authors and tacitly or explicitly by the responsible authorities where the work was carried out.
- if accepted, the article will not be published elsewhere in the same form, in English or in any other language, including electronically, without the written consent of the copyright-holder

CRediT authorship contribution statement

Hans-Joachim Krause: Writing – review & editing, Investigation, Conceptualization. **Jae Chan Jeong:** Software, Investigation, Data curation. **Ali Mohammad Pourshahidi:** Writing – original draft, Software, Methodology, Investigation, Data curation. **Hyo Bong Hong:** Writing – review & editing, Supervision, Project administration, Methodology, Funding acquisition.

Ethics approval and consent to participate

Not applicable

Consent for publication

Not applicable

Funding

This work was supported in part by the Electronics and Telecommunications Research Institute under Grant "25RBG1310".

Declaration of Competing Interest

The authors declare that they have no known competing financial interests or personal relationships that could have appeared to influence the work reported in this paper.

Appendix A. Supporting information

Supplementary data associated with this article can be found in the online version at doi:10.1016/j.sna.2025.117095.

Data availability

Data will be made available on request.

References

[1] P. Liu, P. Jonkheijm, L.W.M.M. Terstappen, M. Stevens, Magnetic particles for CTC enrichment, Cancers 12 (2020) 3525, https://doi.org/10.3390/cancers12123525.
[2] A. Abuawad, Y. Ashhab, A. Offenhäusser, H.-J. Krause, DNA sensor for the detection of brucella spp. Based on magnetic nanoparticle markers, Int. J. Mol. Sci. 24 (2023) 17272, https://doi.org/10.3390/ijms242417272.

[3] P. Farinha, J.M.P. Coelho, C.P. Reis, M.M. Gaspar, A comprehensive updated review on magnetic nanoparticles in diagnostics, Nanomaterials 11 (2021) 3432, https://doi.org/10.3390/nano11123432.
[4] N. Panagiotopoulos, R.L. Duschka, M. Ahlborg, G. Bringout, C. Debbeler, M. Graeser, C. Kaethner, K. Lüdtke-Buzug, H. Medimagh, J. Stelzner, et al., Magnetic particle imaging. Current developments and future directions, Int. J. Nanomed. 10 (2015) 3097–3114, https://doi.org/10.2147/IJN.S70488.
[5] A. Avasthi, C. Caro, E. Pozo-Torres, M.P. Leal, M.L. García-Martín, Magnetic nanoparticles as MRI contrast agents, Top. Curr. Chem. Cham 378 (2020) 40, https://doi.org/10.1007/s41061-020-00302-w.
[6] S.M. Dadfar, D. Camozzi, M. Darguzyte, K. Roemhild, P. Varvarà, J. Metselaar, S. Banala, M. Straub, N. Güvener, U. Engelmann, et al., Size-Isolation of superparamagnetic iron oxide nanoparticles improves MRI, MPI and hyperthermia performance, J. Nanobiotechnology 18 (2020) 22, https://doi.org/10.1186/s12951-020-0580-1.
[7] Magnetic Particle Imaging: A Novel SPIO Nanoparticle Imaging Technique; Buzug, T.M., Borgert, J., Eds.; Springer proceedings in physics; Springer: Heidelberg, 2012; ISBN 978-3-642-24132-1..
[8] U.M. Engelmann, J.L. Fitter, M. Baumann, Assessing magnetic fluid hyperthermia: magnetic relaxation simulation, modeling of nanoparticle uptake inside pancreatic tumor cells and in vitro efficacy, Infinite Science Publishing, 2019.
[9] Z. Hedayatnasab, F. Abnisa, W.M.A.W. Daud, Review on magnetic nanoparticles for magnetic nanofluid hyperthermia application, Mater. Des. 123 (2017) 174–196, https://doi.org/10.1016/j.matdes.2017.03.036.
[10] R. Pala, S. Pattnaik, S. Busi, S.M. Nauli, Nanomaterials as novel cardiovascular theranostics, Pharmaceutics 13 (2021) 348, https://doi.org/10.3390/pharmaceutics13030348.
[11] S. Balaban Hanoglu, D. Harmanci, N. Ucar, S. Evran, S. Timur, Recent approaches in magnetic Nanoparticle-Based biosensors of miRNA detection, Magnetochemistry 9 (2023) 23, https://doi.org/10.3390/magnetochemistry9010023.
[12] Y.-T. Chen, A.G. Kolhatkar, O. Zenasni, S. Xu, T.R. Lee, Biosensing using magnetic particle detection techniques, Sensors 17 (2017) 2300, https://doi.org/10.3390/s17102300.
[13] J.B. Haun, T.-J. Yoon, H. Lee, R. Weissleder, Magnetic nanoparticle biosensors, WIREs Nanomed. Nanobiotechnology 2 (2010) 291–304, https://doi.org/10.1002/wnan.84.
[14] S. Ota, Y. Takemura, Characterization of Néel and brownian relaxations isolated from complex dynamics influenced by dipole interactions in magnetic nanoparticles, J. Phys. Chem. C. 123 (2019) 28859–28866, https://doi.org/10.1021/acs.jpcc.9b06790.
[15] F. Ludwig, H. Remmer, Rotational dynamics of magnetic nanoparticles in different matrix systems, Phys. Sci. Rev. 7 (2022) 981–1008, https://doi.org/10.1515/psr-2019-0115.
[16] JohannaS34 Low Cost Bench Top Magnetic Particle Spectrometer (MPS) Available online: ⟨https://www.instructables.com/Low-Cost-Bench-Top-Magnetic-Particle-Spectrometer-/⟩ (accessed on 17 April 2024).
[17] Wu, K.; Chugh, V.K.; di Girolamo, A.; Liu, J.; Saha, R.; Su, D.; Krishna, D.; Nair, A.; Davies, W.; Wang, A.Y.; et al. Portable Magnetic Particle Spectrometer (MPS) for Future Rapid and Wash-Free Bioassays. 26.
[18] S. Rettcher, F. Jungk, C. Kühn, H.-J. Krause, G. Nölke, U. Commandeur, R. Fischer, S. Schillberg, F. Schröper, Simple and portable magnetic immunoassay for rapid detection and sensitive quantification of plant viruses, Appl. Environ. Microbiol 81 (2015) 3039–3048, https://doi.org/10.1128/AEM.03667-14.
[19] Y. Liu, X. Feng, S. Liu, L. Li, X.-Y. Huang, M. He, C.-F. Qin, H. Hui, J. Tian, Peak shift in Field-Swept magnetic particle spectroscopy: a novel sensing metric for magnetic nanoparticle bioassays, IEEE Trans. Instrum. Meas. 73 (2024) 1–10, https://doi.org/10.1109/TIM.2024.3436100.
[20] Z. Du, G. Zhao, Z. Hua, N. Ye, Y. Sun, W. Wu, H. Zhang, L. Yu, S. Han, H. Wang, et al., A novel estimation method for temperature of magnetic nanoparticles dominated by brownian relaxation based on magnetic particle spectroscopy, IEEE Trans. Instrum. Meas. 73 (2024) 1–16, https://doi.org/10.1109/TIM.2024.3472772.
[21] F.T. Wolgast, T. Kahmann, K.-J. Janssen, T. Yoshida, J. Zhong, M. Schilling, F. Ludwig, T. Viereck, Low-Cost magnetic particle spectroscopy hardware for Low-Viral-Load immunoassays, IEEE Trans. Instrum. Meas. 73 (2024) 1–9, https://doi.org/10.1109/TIM.2024.3449985.
[22] B. Tian, T.Z.G. de la Torre, M. Donolato, M. Fougt Hansen, P. Svedlindh, M. Strömberg, Multi-Scale magnetic nanoparticle based optomagnetic bioassay for sensitive DNA and bacteria detection, Anal. Methods 8 (2016) 5009–5016, https://doi.org/10.1039/C6AY00721J.
[23] B. Gil Rosa, O.E. Akingbade, X. Guo, L. Gonzalez-Macia, M.A. Crone, L.P. Cameron, P. Freemont, K.-L. Choy, F. Güder, E. Yeatman, et al., Multiplexed immunosensors for Point-of-Care diagnostic applications, Biosens. Bioelectron. 203 (2022) 114050, https://doi.org/10.1016/j.bios.2022.114050.
[24] A.W. Wark, H.J. Lee, R.M. Corn, Multiplexed detection methods for profiling MicroRNA expression in biological samples, Angew. Chem. Int. Ed. 47 (2008) 644–652, https://doi.org/10.1002/anie.200702450.
[25] A. Malhotra, A. Von Gladiss, A. Behrends, T. Friedrich, A. Neumann, T.M. Buzug, K. Lüdtke-Buzug, Tracking the growth of superparamagnetic nanoparticles with an In-Situ magnetic particle spectrometer (INSPECT), Sci. Rep. 9 (2019) 10538, https://doi.org/10.1038/s41598-019-46882-6.
[26] D. Hautot, Q.A. Pankhurst, N. Khan, J. Dobson, Preliminary evaluation of nanoscale biogenic magnetite in Alzheimer's disease brain tissue, Proc. Biol. Sci. 270 (2003) S62–S64.
[27] A.M. Rauwerdink, A.J. Giustini, J.B. Weaver, Simultaneous quantification of multiple magnetic nanoparticles, Nanotechnology 21 (2010) 455101, https://doi.org/10.1088/0957-4484/21/45/455101.
[28] Wu, K.; Saha, R.; Su, D.; Dk, V.; Liu, J.; Cheeran, M. *Magnetic Immunoassays: A Review of Virus and Pathogen Detection Before and Amidst the Coronavirus Disease-19 (COVID-19)*; 2020;
[29] K. Wu, V.K. Chugh, V. D. Krishna, A. di Girolamo, Y.A. Wang, R. Saha, S. Liang, M. C.-J. Cheeran, J.-P. Wang, One-Step, Wash-Free, nanoparticle Clustering-Based magnetic particle spectroscopy bioassay method for detection of SARS-CoV-2 spike and nucleocapsid proteins in the liquid phase, ACS Appl. Mater. Interfaces 13 (2021) 44136–44146, https://doi.org/10.1021/acsami.1c14657.
[30] M.H.F. Meyer, M. Hartmann, H.-J. Krause, G. Blankenstein, B. Mueller-Chorus, J. Oster, P. Miethe, M. Keusgen, CRP determination based on a novel magnetic biosensor, Biosens. Bioelectron. 22 (2007) 973–979, https://doi.org/10.1016/j.bios.2006.04.001.
[31] H.-B. Hong, Detection of two different influenza a viruses using a nitrocellulose membrane and a magnetic biosensor, J. Immunol. Methods 6 (2011).
[32] K. Wu, J. Liu, R. Saha, D. Su, V.D. Krishna, M.C.-J. Cheeran, J.-P. Wang, Magnetic particle spectroscopy for detection of influenza a virus subtype H1N1, ACS Appl. Mater. Interfaces 12 (2020) 13686–13697, https://doi.org/10.1021/acsami.0c00815.
[33] S. Achtsnicht, A.M. Pourshahidi, A. Offenhäusser, H.-J. Krause, Multiplex detection of different magnetic beads using frequency scanning in magnetic frequency mixing technique, Sensors 19 (2019) 2599, https://doi.org/10.3390/s19112599.
[34] L. Tu, K. Wu, T. Klein, J.-P. Wang, Magnetic nanoparticles colourization by a Mixing-Frequency method, J. Phys. Appl. Phys. 47 (2014) 155001, https://doi.org/10.1088/0022-3727/47/15/155001.
[35] A.M. Pourshahidi, S. Achtsnicht, M.M. Nambipareechee, A. Offenhäusser, H.-J. Krause, Multiplex detection of magnetic beads using offset field dependent frequency mixing magnetic detection, Sensors 21 (2021) 5859, https://doi.org/10.3390/s21175859.
[36] T. Bikulov, F. Eivazi, A. Offenhäusser, H.-J. Krause, Multicontrasting MPS by dual-tone nonlinearity probing, Int. J. Magn. Part. Imaging IJMPI 10 (2024), https://doi.org/10.18416/IJMPI.2024.2403014.
[37] S.-M. Choi, J.-C. Jeong, J. Kim, E.-G. Lim, C. Kim, S.-J. Park, D.-Y. Song, H.-J. Krause, H. Hong, I.S. Kweon, A novel Three-Dimensional magnetic particle imaging system based on the frequency mixing for the Point-of-Care diagnostics, Sci. Rep. 10 (2020) 11833, https://doi.org/10.1038/s41598-020-68864-9.
[38] Krause, H.-J.; Engelmann, U.M. Fundamentals and Applications of Dual-Frequency Magnetic Particle Spectroscopy: Review for Biomedicine and Materials Characterization. *Adv. Sci. n/a*, 2416838, ⟨doi:10.1002/advs.202416838⟩.
[39] T. Bikulov, M.-B. Abbas, H.-J. Krause, A. Offenhäusser, U. Engelmann, Dual-Frequency MPS enables direct MNP size reconstruction: verification with micromagnetic simulation data, Int. J. Magn. Part. Imaging IJMPI 11 (2025), https://doi.org/10.18416/IJMPI.2025.2503005.
[40] V.K. Chugh, S. Liang, P. Yari, K. Wu, J.-P. Wang, A method for multiplexed and volumetric-based magnetic particle spectroscopy bioassay: mathematical study, J. Phys. Appl. Phys. 56 (2023) 315001, https://doi.org/10.1088/1361-6463/acd0bd.

Dr. A.M. Pourshahidi is a PostDoctoral Researcher at Forschungszentrum Jülich. His main research topics are Magnetic Tweezers, Frequency Mixing Magnetic Detection.

Dr. J. J. Jeong is a senior researcher at the Electronics and Telecommunications Research Institute (ETRI). His primary research interests include software and equipment development related to nanomagnetic particle analysis and imaging equipment.

Prof. Dr. H-J Krause is a Professor of Physics at FH Aachen University of Applied Sciences and Principal Investigator at Forschungszentrum Jülich. He leads the Magnetic Field Sensors group, focusing on magnetic biosensing, magnetic immunoassays with frequency mixing magnetic detection, and low-field nuclear magnetic resonance.

Dr. Hong is a Department Director and Principal Researcher at the Electronics and Telecommunications Research Institute (ETRI). His research focuses primarily on the analysis of nanomagnetic particles and the development of imaging equipment.